Venkatesh, M., Gouthaman, S., Kanemoto, S. O., Lakshmi, M. S., & Hamerton, I. (2019). Development of epoxy-cyanate ester-clay nanocomposites offering enhanced thermal stability. *Journal of Applied Polymer Science*, *136*(28), [47754]. https://doi.org/10.1002/app.47754

Development of Epoxy-Cyanate Ester-Clay Nanocomposites Offering Enhanced Thermally Stability

M. Venkatesh[a], S. Gouthaman[a], S.O. Kanemoto[a,b], M.S. Lakshmi[a], I. Hamerton,[c]*

[a] *Polymer Science & Technology Division, Central Leather Research Institute (CSIR – CLRI), Chennai, 600 020, India*.
[b] *Macromolecular Research Team, Department of Inorganic Chemistry, University of Yaounde-I, 812-Yaounde, Cameroon*
[c] *Bristol Composites Institute (ACCIS), School of Civil, Aerospace, and Mechanical Engineering, Queen's Building, University of Bristol, University Walk, Bristol, BS8 1TR, U.K.*

* Correspondence to Prof. Ian Hamerton,
E.mail : ian.hamerton@bristol.ac.uk, Tel. : +44-(0)117-3314799.

Abstract

The preparation and characterization of blends of a series of dicyanate monomers: 2,2'-*bis*(4-cyanatophenyl) propane (DCDPP), *bis*-4-cyanato-biphenyl (DCBP), *bis*-4-cyanatonaphthalene (DCN), 3,3'-*bis*(4-cyanatophenyl)sulphide (DCTDP), and 3,3'-*bis*(4-cyanatophenyl)sulphone (DCDPS), and the diglycidyl ether of bisphenol A, is reported. These copolymers are combined with a Montmorillionite nanoclay and both epoxy-cyanate blends and epoxy-cyanate blends-nanoclay composites are all analysed for thermal stability, thermal degradation kinetics, flame retardancy, and impact strength. The nanocomposites are further characterized by x-ray diffraction and SEM to determine morphological features, from which structure-property relationships are determined. Dispersion of the nanoclay is of paramount importance, but its inclusion serves to improve char yield and impact strength, when this is achieved.

1. Introduction

Conventional epoxies are not suitable to satisfy many high performance applications, due to their inherent brittleness and limitations in thermal/thermo-oxidative stability and poor hot/wet performance. Consequently, several approaches have been tried to improve those

characteristics.[1-6] For instance, fracture toughness enhancement has typically been imparted through the incorporation of various thermoplastic polymers,[7-11] but this can impact deleteriously on some of the key physical properties such as glass transition temperature, moisture resistance, and viscoelastic behaviour.[12-15] Alternatively, the properties can be enhanced by use of the tailored epoxy (Ep) backbones (*e.g.* incorporating higher functionality or greater aromaticity), by using chemically modified curing agents, or using high performance co-monomers such as cyanate esters and/or bismaleimides (BMIs) as additives.[16] Bismaleimides networks are usually brittle due to the high cross-link density of the structure. Consequently, cyanate esters (Cy) have definite advantages over BMIs due to the lower crosslink density and higher flexibility in the final polymer network, arising from the high percentage of oxygen linkages present.[17,18] When incorporated into an epoxy copolymer, these attributes of cyanate esters are reflected in higher fracture toughness and lower modulus when compared to BMI resins.[19,20] The relatively high price of the cyanate esters is one of the main barriers to their wider adoption in many technologies in which their extremely low dielectric constant and low dielectric loss properties make them potentially very applicable.[21] Thus, in the search to achieve superior performance, coupled with reduction in cost, cyanate-modified epoxy resins offer an attractive family of hybrids with many of the beneficial properties shared by both homopolymers.[22] These drawbacks could be surmounted by developing formulations using nanoclays, which are relatively cheap and which are expect to yield competitive performance characteristics.[23-24]

Many of the aforementioned high-performance resins and their formulations were not been effectively utilized during the past have now become feasible for making unique, specific and customized components.[25-30]

Considering high-rise in proximity of employing these resins in emerging technologies for making very high performance oriented materials, we have researched on synthetic methodology and attributes of several cyanate esters, inorder to make available to the researcher community to exploit it to find several other arenas. Therefore, cyanate ester resins with different rigid backbones were prepared and they mixed with epoxy and further combined with nanoclay to produce nanocomposites. They were subjected to systematic investigations, to establish the properties with a view to investigate the influence of cyanate in epoxy and in epoxy/nanoclay blends in terms of the thermal stability and toughening properties in epoxy resins.

2. Experimental

2.1. Materials

The diglycidylether of bisphenol A (DGEBA, LY556, EEW 180-185 g/mol., density 1.23 g/cm^3, refractive index 1.57 and viscosity 10,000 cP) (Fig. 1) was supplied by Ciba Speciality Chemicals PVT Ltd., India, 4,4-diaminodiphenylsulphone (DDS) was procured from Fluka Company and triethylamine from the Aldrich Company. Nanomer 1.30E (a Montmorillonite, MMT-clay furnace modified with octadecylammonium halide) was also obtained from Aldrich and used as received. 2,2-B*is*(4-hydroxylphenyl) propane; 4,4′-dihydroxybiphenyl; 2,7-dihydroxynaphthalene; bis(4-hydroxyphenyl)sulfide and bis(4-hydroxyphenyl)sulfone were purchased from Aldrich, all with purity ≥97%.

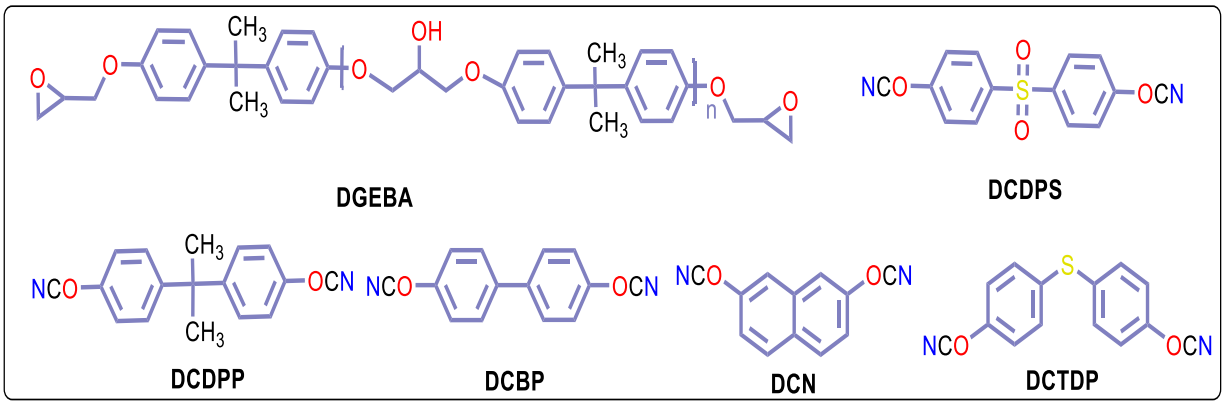

Fig. 1. Structures of the monomers studied in this work

2.2. Analytical Methods

FT-IR spectra were recorded on a PerkinElmer Spectrum Two IR spectrometer, in the range from 4000 to 400 cm^{-1} with 12 scans at a resolution of 4 cm^{-1}. The microstructures of epoxy-cyanate (Ep-Cy) blends and epoxy-cyanate-nanoclay (Ep-Cy-Nc) blends were characterized using scanning electron microscopy using a JEOL JSM-6320F SEM (JEOL USA, Inc.). The thermal stabilities of the prepared nanocomposites (10-15 mg) were determined using a TGA Q50-TA thermal analyzer from 30-800°C using alumina crucibles at a heating rate of 10 K per minute under nitrogen atmosphere with the flow rate of 60 ml per minute. The X-ray diffraction studies were carried out using a Rigaku Miniflex Japan, at an operating voltage of 40 kV and current of 30 mA with CuKa1 radiation (wavelength = 1.54056 Å), in the region of 2Θ from 10º to 80º.

2.3. Synthesis of cyanate ester monomers

A batch scale of DCDPP cyanate ester (100 g) was synthesized at 0°C (maintained using an cooling bath, containing a mixture of NaCl and ice) by the reaction of cyanogen bromide and bisphenol A in the presence of triethylamine as a base (slow, dropwise addition of the reagents to maintain the temperature and using a slight excess of trimethylamine) based on a well-used route, originally reported by Grigat and Pütter (of Bayer AG).[31,32] Following the addition of the reagents, the mixture was stirred for a further 60 minutes and allowed to reach room temperature

before the aqueous work up was performed to isolate the DCDPP monomer. The syntheses of the other cyanate ester monomers (DCBP, DCN, DCTDP, and DCDPS) were prepared from their respective dihydroxy compounds by employing the same procedure. Yields based on the addition of the limiting reagent, cyanogen bromide, were typically ≈81 %.

2.3.1. Preparation of Ep-Cy blends

The Ep-Cy contains solely DGEBA, the corresponding dicyanate, and the DDS curing agent in stoichiometric ratio to the DGEBA. Thus, into the DGEBA-DDS stock taken in a stoichiometric ratio, was blended each dicyanate (DCDPP, DCBP, DCN, DCTDP, and DCDPS) as shown in Table 1, along with the curing conditions. Thus, the blends of DGEBA with DDS were made by employing the compositions in the same equivalent ratios. Thus, to a blend comprising 100wt%, was added cyanate (10 wt%). The blends were mixed thoroughly at 120°C in an oil bath to get a homogeneous liquid. When the formulations were melted and became homogeneous they were transferred to a preheated open mould that was coated with silicon based release agent. The mold was preheated to 120°C before transferring the formulations. After the material was transferred to the mould it was heated to 130°C and degassed under vacuum for 0.5h. All the formulations were heated to 140°C and held isothermally for 3h, 160°C for 2h and 180°C for 3h. Then the cured laminates were removed from the mould and curing was continued at180°C for 2h. The cured samples were made cut to suitable dimensions required for the characterization of its physical, chemical, thermal, and mechanical properties.

Table 1. Samples specifications

Sample code	DGEBA* (wt%)	DGEBA-Cyanate (Ratio w/w)	Nanoclay (wt%)	Curing		Post Curing	
				1	2	1	2
Ep-Cy	100	10	0	140°C for 3h	160°C for 2h	180°C for 4h	200°C for 2h

Ep-Cy-Nc	100	10	5	140°C for 3h	160°C for 2h	180°C for 4h	200°C for 2h

* Diaminodiphenyl sulfone (DDS) curing agent was added at the stoichiometric ratio to DGEBA

2.3.2. Preparation of Ep-Cy-Nc nanocomposites systems

The Ep-Cy-Nc systems all contained DGEBA, the corresponding dicyanate, and MMT clay. Thus, the DGEBA-DDS stock blend was considered as 100 wt% and to individual samples of this stock was added a dicyanate (DCBP, DCDPS, DCDPP, DCN, DCTDP in quantities shown in Table 1). A predefined amount of nanoclay was placed in a 250 ml beaker containing 100 ml acetone and stirred to facilitate the dispersion of nanoclay. The clay dispersion was sonicated for 4h. To the clay dispersion, DGEBA was added and stirred at room temperture. When a homogeneous dispersion had been achieved, the solvent was removed by rotary evaporator and transferred to a 100 ml round bottom flask and to the DGEBA was added cyanate (10 wt%), followed by DDS in a stoichiometric ratio based on the DGEBA content.

The nanoclay dispersion thus obtained with DGEBA-DDS-Cy mixture was kept in an oil bath which was preheated at 90°C and was stirred slowly until it became transparent. The resulting prepolymer was poured into a stainless steel mould that had been preheated to 140°C and cured at different temperatures as given in 2.3.1.

3. Results and Discussion

It is well established that the inclusion of well-dispersed nanoclays serves to reinforce organic matrices and a schematic representation of the cured Ep-Cy molecules intercalated within the gallery regions of the nanoclay is shown in Fig. 2.

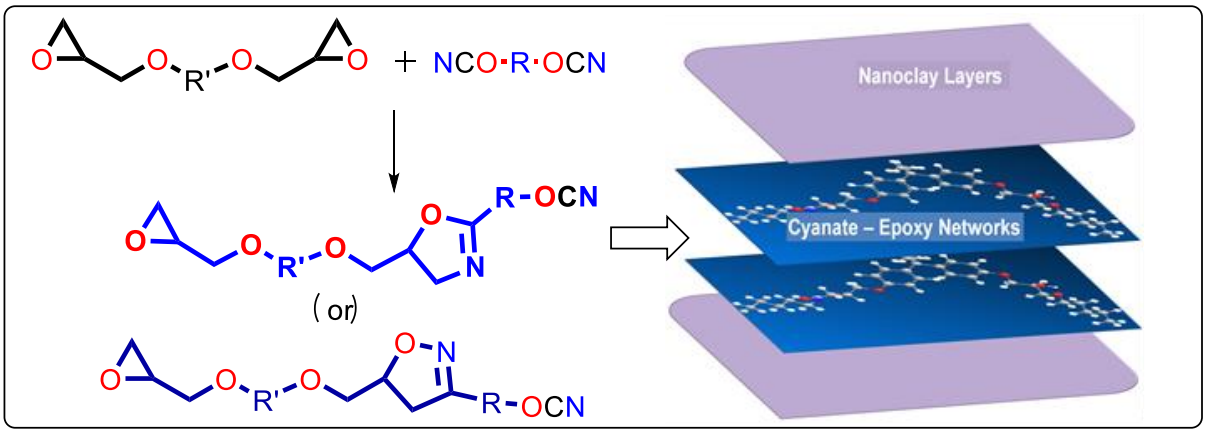

Fig. 2. A schematic representation of the epoxy/cyanate (Ep-Cy) cured molecules intercalated in the nanoclay layers.

Simplified structures of the copolymers are shown (particularly the oxazolidinone),[33] since previous studies by Shimp *et al.*[34] and Bauer *et al.*[35,36] studying the cyanate-epoxy co-reaction mechanism using either model compounds (4-chlorophenylcyanate and phenylglycidylether) or difunctional compounds (DCDPP and DGEBA) identified a number of general points: the only significant parameters that influences the reaction products are temperature and the catalyst, Bauer and collaborators found that the atmosphere and the stoichiometric ratio do not alter the reaction path, but only the relative proportions of the reaction products. The reaction has been proposed to proceed *via* six main steps (Fig. 3) and (a)-(d) are believed to predominate:

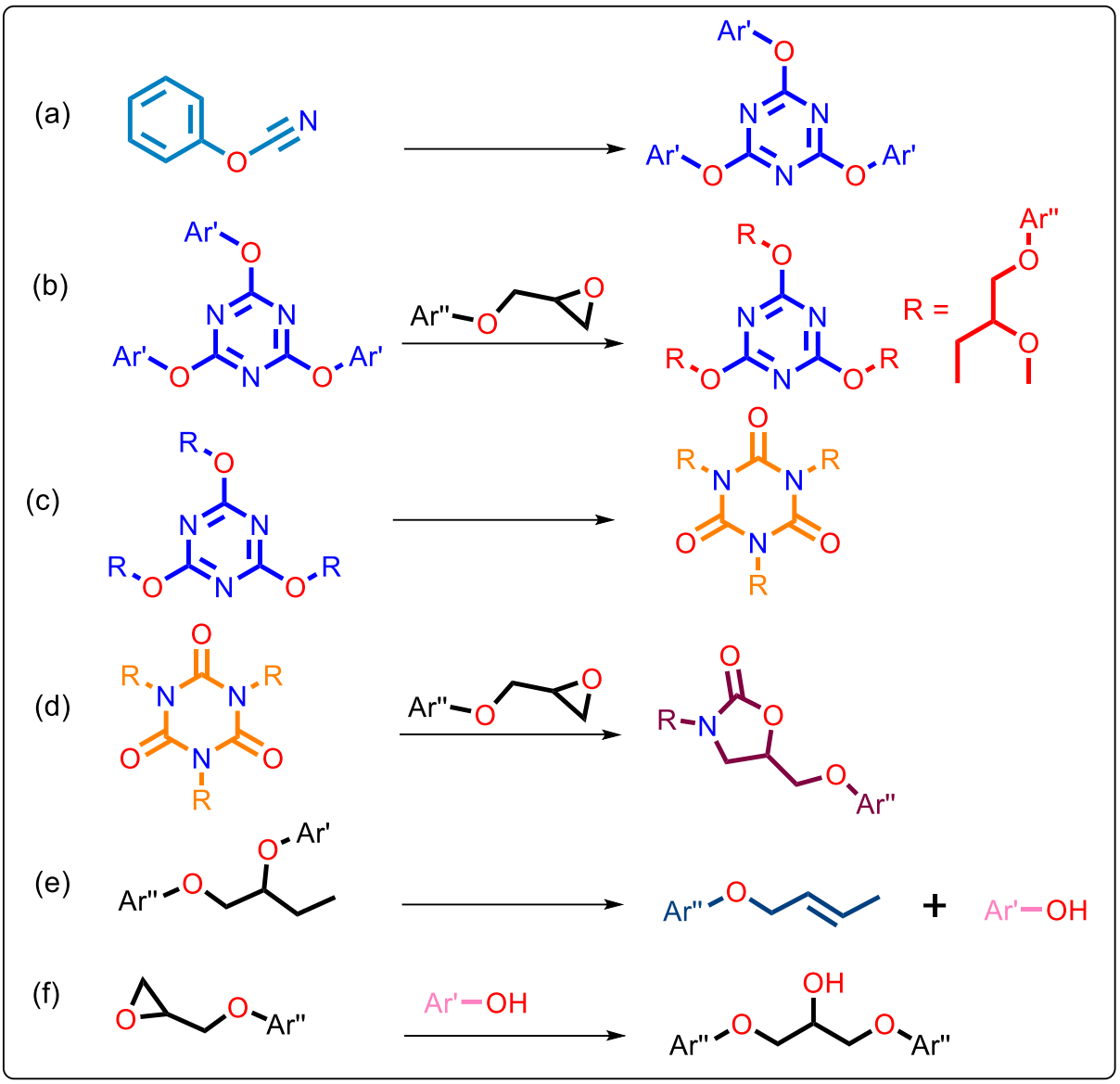

Fig. 3. Accepted reaction mechanism for the epoxy-cyanate (Ep-Cy) co-reaction (note these are not sequential)

FT-IR spectra (Fig. 4) have shown the total conversion of cyanate function group (O-C≡N) in the films composites due to the absence of the characteristic O-C≡N stretching peak in the region of 2200 cm^{-1}. The broad peak around 3400-3300 cm^{-1} is attributed to aliphatic and aromatic hydroxyl (O-H) groups. The characteristic peaks of 2950-2880 cm^{-1} (C-H stretch), 1740 cm^{-1} (C=O stretch), 1580-1490 cm^{-1} (aromatic C=C and C-N stretches) show clearly the progress of the chemical reaction during the curing process of the films.

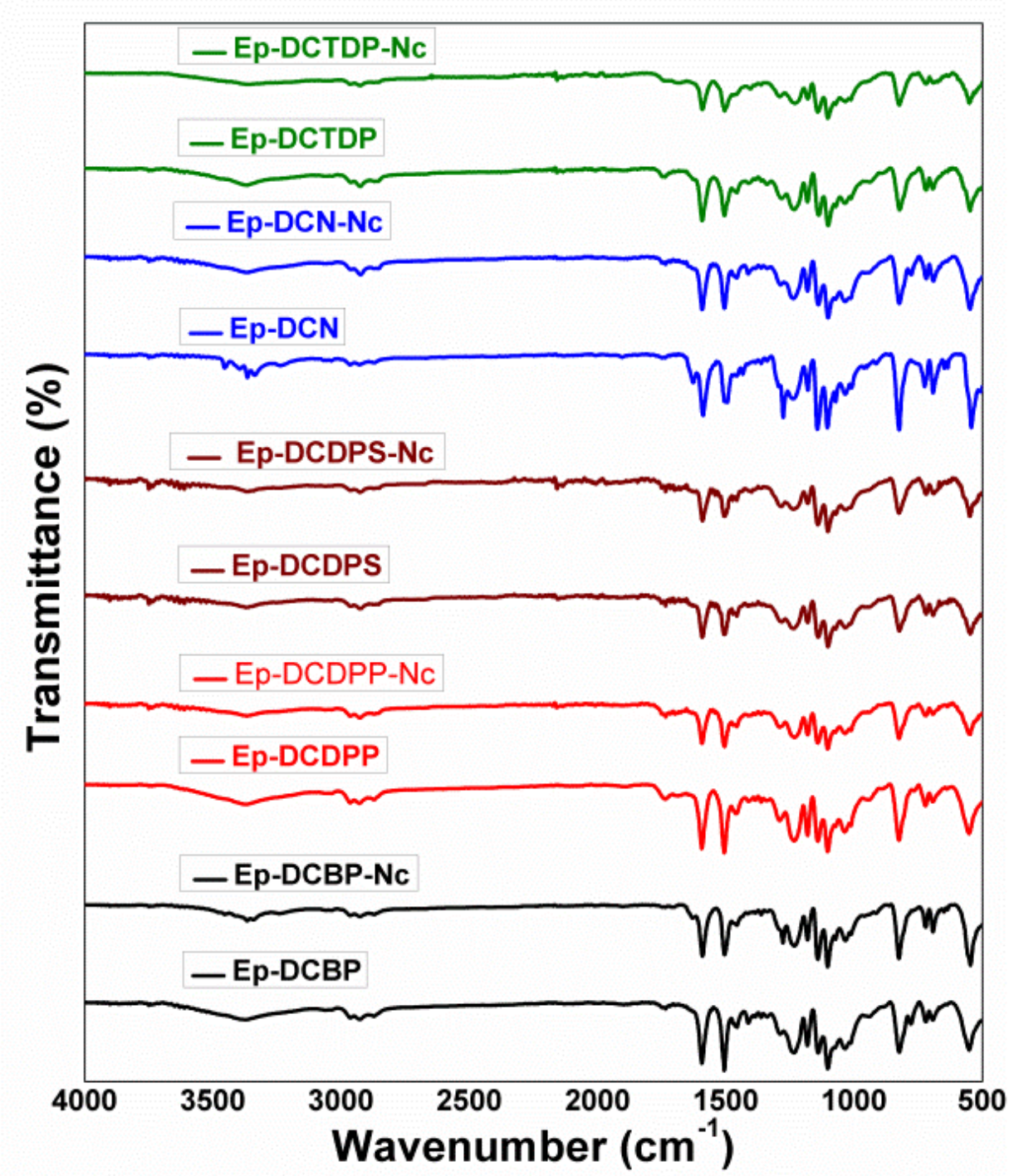

Fig. 4. FT-IR spectra of the cured samples of DGEBA-cyanate blends Ep-Cy and DGEBA-cyanate blends with clay Ep-Cy-Nc

3.1. X-ray Diffraction (XRD) analysis

Wide angle X ray diffraction (WAXD) methods were employed to examine the long range order. The XRD patterns of organonanoclay (Nc) and the Ep-Cy-Nc systems prepared with

MMT nanoclays (5 wt%) loading are shown in Fig. 5, from which it can be observed that the pure MMT organoclay (1.30E) displays a peak (d001) at ~ 6° (2θ). In contrast, the scans of the Ep-Cy-Nc systems show no peaks corresponding to the nanoclay 1.30E; the absence of this peak corresponding to (001) plane in WAXD scans might be due to loss of ordered structure during melt processing. The delaminated structure or loss of ordered structure was probably due to the high level of shearing during sonication for 5h followed by 4h of mechanical stirring; this finding is in agreement with the reports of Qiu *et al.*[37]

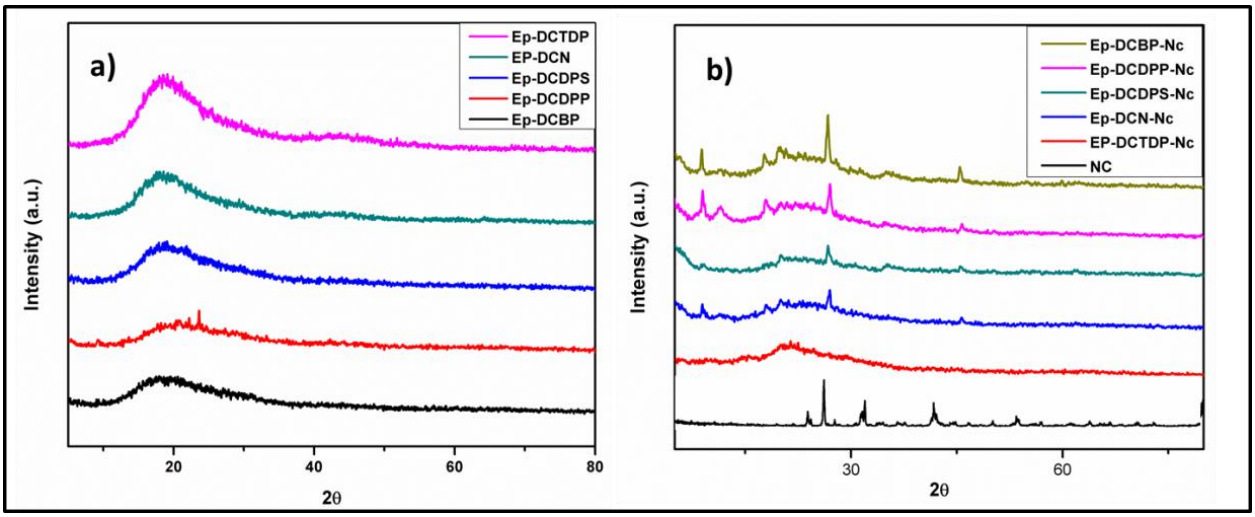

Fig. 5. XRD graph of Ep-Cy (a) and effect of organoclay loading on the structure of Ep-Cy-Nc (b) systems.

3.2. Thermal polymerization behaviour of the blends and nanocomposites

The thermal behaviour of the cured samples of Ep-Cy and Ep-Cy-Nc was studied from the DSC are shown in Fig. 6. All of the cured samples show values of T_g greater than the base epoxy resin (DGEBA-DDS), but the influence of the MMT nanoclay in modifying the T_g is disappointing as there are no significant differences in the T_g found for Ep-DCDPP-Nc and Ep-DCBP-Nc (while Ep-DCN-Nc experiences a fall of 19°C, and Ep-DCTDP 27°C) after modification. The notable exception is Ep-DCDPS-Nc, as the T_g rises by 27°C after modification, from which it is assumed that the presence of the organoclay in the intercalated

state appears to have restricted the mobility with a concomitant increase in the T_g. Given that that the bridging group in the monomer is the most polar of those studied, it may be that this has served to assist the level of dispersion of the nanoclay, and hence the elevation in T_g.

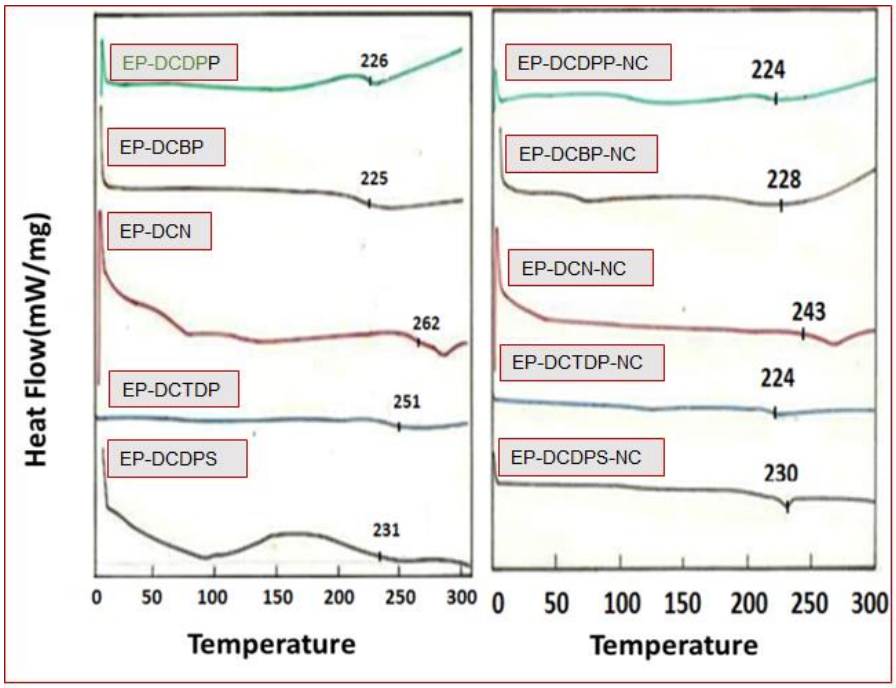

Fig. 6. DSC curves of the cured samples of Ep-Cy and Ep-Cy-Nc blends

3.3. Estimation of crosslink density using DSC data

The estimation of molecular weights between adjacent crosslinks (M_c) helps to understand the physical network structure of the polymer since the parameter is inversely proportional to the crosslink density (Fig. 7).[38] The latter is one of the key structural parameters that aids understanding of changes in the segmental motions, which is reflected in the mechanical properties of the thermoset polymers. When the number of crosslink junctions is increased, the crosslink density also increases along with T_g, and therefore the relationships between T_g and M_c, could be correlated with the cross-link density of the polymer. A qualitative estimation of M_c in both the Ep-Cy-Nc and Ep-Cy systems can be obtained using the empirical equation (1)

$$Mc = \frac{3.9 \times 10^4}{Tg - Tg^0} \quad (1)$$

where Tg^0 is the glass transition temperature of the noncrosslinked polymer.

When the nanocomposites were compared, only Ep-DCDPP-Nc, Ep-DCN-Nc, and Ep-DCTDP-Nc display increased M_c values.

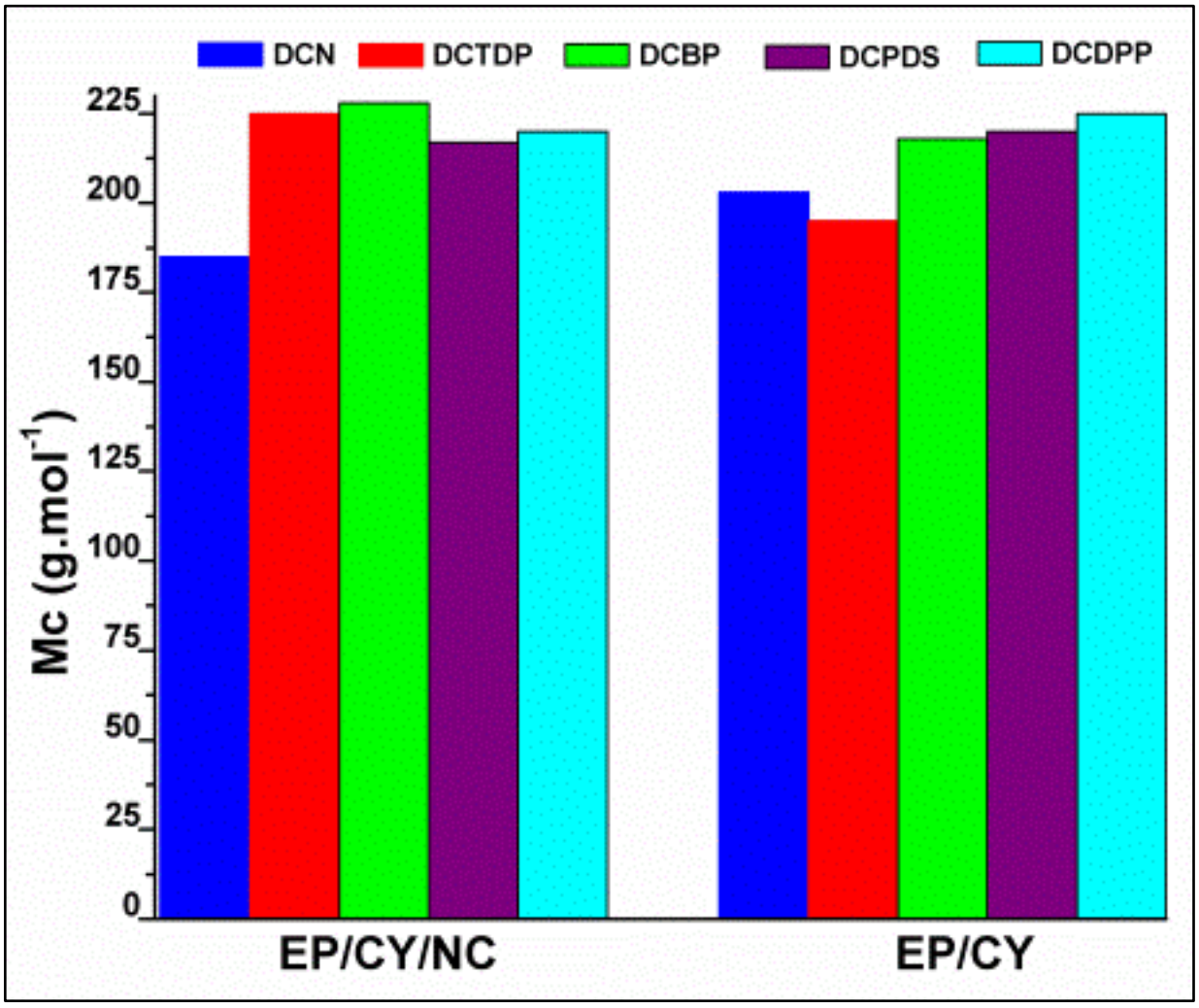

Fig. 7. Correlation between T_g and Molecular weight between the crosslinks (M_c).

Similarly, the Ep-Cy-Nc systems may also have exhibited higher M_c values because of the clay layers present between the crosslink points, but the variations in the M_c values observed suggest that the increase or decrease in crosslink density was not only dependent on the distance or the

molecular weight between the crosslinks, but also on the physical characteristics of the structural backbones and polarity of the functionalities in the segments.

This series of monomers has been chosen to exemplify both a range of backbone polarities: DCDPS > DCTDP > DCN ≈ DCBP > DCDPP and also rotational freedom between aromatic moieties ranging from the most rigid (DCN) where the aromatic rings are fused, biphenyl with limited rotation, through to the less hindered sulphide in which the C-S bonds have mainly sigma character, but with a contribution from the *pi*-bonds of the phenyl rings undergoing interaction with the lone electron pairs on the sulphur atom. Howlin *et al.*[39] previously used molecular simulation methods to explore the rotational freedom of sulphone, ether, and isopropylidene bridges within oligosulphones, and reported energy barriers of rotation of sulphone (1 kcal/mol) < ether = carbonyl (4 kcal/mol) <isopropylidene (6 kcal/mol); in the present series, the thioether link may be considered analogous to the ether, albeit with a significantly larger atomic radius. The rotational freedom of the backbone may influence the degree of conversion achieved, with more flexible links facilitating the movement of (co)reactive functional groups into closer proximity, otherwise hindered by more rigid monomeric structures.

3.4. Determination of thermal stability using thermogravimetic analysis

The thermal stabilities of the cured resin systems were examined using the thermogravimetric analysis (TGA) technique by estimating the initial decomposition temperature (IDT), at which approximately 5% of the sample mass has been lost and where the detectable quantity of heat had been evolved. Also, the onset degradation temperature at which the maximum rate of mass loss (T_{max}) begins and the char yield at which the degradation of the entire sample was complete. The influence of the nanoclay on the thermal stability of the blends was then compared.

3.4.1 Thermal degradation of the cured Ep-Cy blends

The TGA curves of cured samples of the Ep-Cy systems are shown in Fig. 8 (a), with the exception of Ep-DCBP, all display similar profiles (Ep-DCBP surprisingly displays a lower temperature for the initial degradation step around 340°C). The maximum decomposition temperature occurs around 400°C for all of the systems, which illustrated that these composites possess good thermal stabilities. With the exception of Ep-DCBP (containing the biphenyl moiety), all display a single step decomposition, achieving char yields of around 10% (at 800°C). When comparing the char yields, these are broadly in line with the aromatic carbon content.[40,41] The Ep-Cy cyanate monomers display comparatively high initial decomposition temperatures (IDT), with a marginally higher value recorded for Ep-DCDPS, and a significantly lower value for DCBP. In the case of Ep-DCDPS, previous work has reported the loss of sulphur dioxide at during thermal degradation of polycyanurates[42] and polyaspartimides[43] containing sulphonyl bridges.

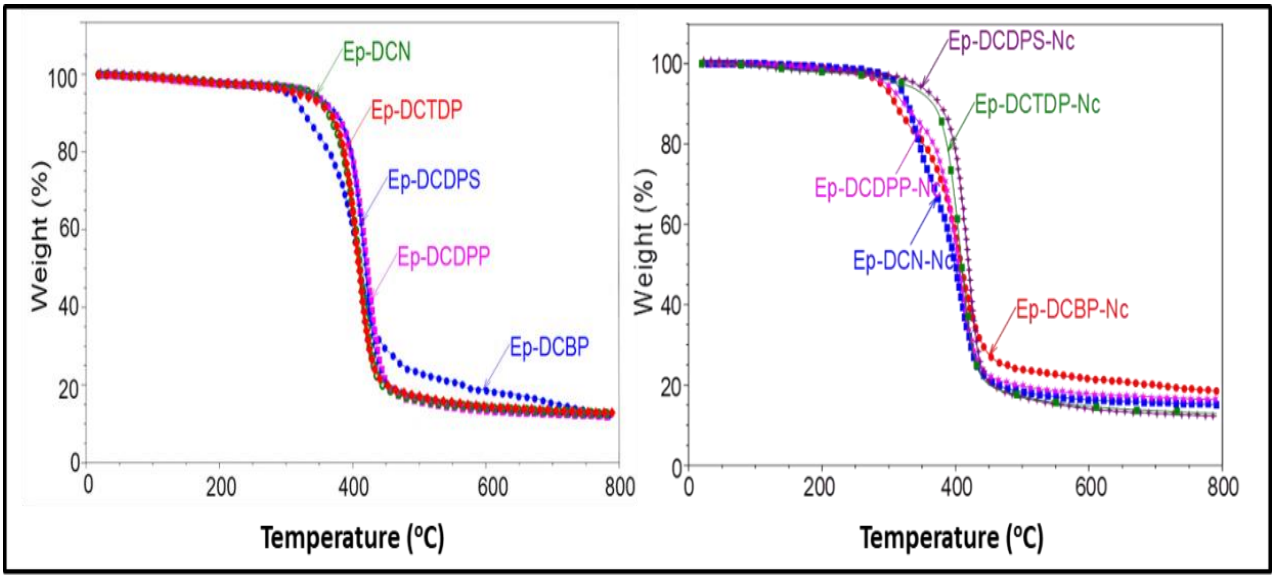

Fig. 8. TGA curves of the Ep-Cy (a) and Ep-Cy-Nc (b) systems carried out under N_2 atmosphere at a heating rate of 10 K/min.

Furthermore, the synergistic effect of oxazolidinone rings, formed through co-reaction of the cyanates with the DGEBA, increase the crosslink density and restrict the segmental motion, which is reflected in increased IDT values. The Ep-Cy systems all exhibit higher char yield values than the conventional epoxy (char yield of DGEBA-DDS is 1.86%),[44] with Ep-DCBP displaying the highest char yield.

3.4.2 Thermal degradation of the cured nanocomposite blends

The TGA curves of cured samples of the Ep-Cy-Nc systems are shown in Figure 8 (b). It is apparent that the addition of the nanoclay effects a change in the profile of the TGA profiles and hence the degradation mechanism; the inclusion of the inorganic nanoclay component understandably increases the char yield of the nanocomposites, with DCBP-Nc showing the highest char yield (Table 1).

Table 1: Thermal properties of the Ep-CY and Ep-Cy/NC systems

Sample	**Initial decomposition temperature (˚C)**	**Final decomposition temperature**	**Char yield**	**Max weight loss**
Ep-DCN	340˚C (6% loss)	450˚C (21% remains)	13%	350-450˚C (73%)
Ep-DCTDP	345˚C (6% loss)	450˚C (22% remains)	13%	350-450˚C (72%)
Ep-DCDPS	353˚C (6% loss)	450˚C (22% remains)	12%	350-450˚C (72%)
Ep-DCDPP	353˚C (6% loss)	450˚C (21% remains)	12%	350-450˚C (73%)
Ep-DCBP	295˚C (4% loss)	450˚C (29% remains)	12%	290-450˚C (67%)
Ep-DCN-Nc	305˚C (3% loss)	450˚C (22% remains)	16%	310-450˚C (75%)
Ep-DCTDP-Nc	290˚C (3% loss)	465˚C (22% remains)	14%	310-450˚C (75%)
Ep-DCDPS-Nc	325˚C (3% loss)	465˚C (22% remains)	13%	310-450˚C (75%)
Ep-DCDPP-Nc	275˚C (3% loss)	465˚C (23% remains)	18%	275-450˚C (74%)
Ep-DCBP-Nc	275˚C (3% loss)	465˚C (28% remains)	20%	275-450˚C (69%)

While the TGA trace for DCTDP-Nc shows little change (there is a modest increase in the value of IDT), the other materials display a significantly lower thermal stability with a bimodal profile.

3.4.3 Determination of the IPDT properties for the cured polymers

The thermal stability of the systems was established with the integral procedural temperature (IPDT) studies. The IPDT proposed by Doyle was calculated using Eq. (2) [45]

$$IPDT(°C) = A^{*}K^{*}(T_f - T_i) + T_i \quad (2)$$

where, A* represents the area ratio of total experimental curve divided by total TGA thermogram, K* is the coefficient of A*, T_i is the initial experimental temperature, and T_f is the final experimental temperature.

The IPDT value of both Ep-Cy and Ep-Cy/Nc systems were calculated from the thermograms obtained by decomposing at a constant heating rate of 10 K/min. All the systems exhibit IPDT values around 900°C confirming the high thermal stability of the materials. The IPDT values of all the Ep-Cy systems were found to be in the similar range given the structural similarities between the dicyanates *e.g.* Ep-DCDPP (982), Ep-DCBP (979), Ep-DCN (980), Ep-DCTDP (982), and Ep-DCDPS (1097). The nanocomposites systems which display excellent miscibility with the clay show higher IPDT values: Ep-DCBP-Nc (1114), Ep-DCTDP-Nc (1099), and Ep-DCDPS-Nc (1097), whereas those displaying poorer miscibility show lower IPDT values: Ep-DCN-Nc (930) and Ep-DCDPP-Nc (938).

3.5.3 Determination of the kinetic parameters for the thermal degradation processes

Data acquired from the TGA experiments were used for the determination of the kinetics of thermal degradation of polymers. The thermal degradation of the cured system was carried out at a heating rate of 10 K/min under a flowing nitrogen atmosphere. The activation energy and order of reaction (n) were predicted by the integral methods of using the Broido, Horowitz-Metzger, and Coats-Redfern models[46-48] are shown in Fig. 9, derived from the Arrhenius equation. The basic equation used to describe decomposition reactions is

$$\frac{dy}{dt} = k(T)\, f(y) \tag{3}$$

The rate constant k(T) and f(y) were functions of temperature, and conversion respectively was defined as

$$y = \frac{M_0 - M_t}{M_0 - M_f} \tag{4}$$

where M_0: initial sample weight, M_t and M_f were the weight at time t and final sample weight respectively. Usually k assumed to follow Arrhenius relationship:

$$k = A\exp\left(\frac{-E}{RT}\right) \tag{5}$$

The reaction rate may be written as follows.

$$\frac{dy}{dt} = \frac{dy}{dT}\frac{dT}{dt} = \beta\frac{dy}{dt} \tag{6}$$

Thus, change in mass *vs.* Temperature can be written as

$$\frac{dy}{dT} = \frac{A}{\beta}\exp\left(\frac{-E_a}{RT}\right) f(y) \tag{7}$$

The integral form of Eq.7 from initial temperature, T_i corresponding to a degree of conversion $m_{0,}$ to a peak temperature, T_{max}, can be written as

$$\int_0^y \frac{dy}{f(y)} = \frac{A}{\beta}\int_{T_0}^{T_P} \exp\left(-\frac{E_a}{RT}\right)dT \tag{8}$$

Using an approximation, Broido rearranged the Eq (8).[49]

$$\ln\left[\ln\frac{1}{y}\right] = -\frac{E_a}{R}\frac{1}{T} + \left(\frac{R}{E_a}\frac{A}{\beta}T_{\max}^2\right)_a \quad (9)$$

The Coats-Redfern equation is shown in Eq (10):

$$\ln\left[\frac{-\ln(1-y)}{T^2}\right] = \ln\frac{AR}{\beta E_a}\left(1-\frac{2RT}{E_a}\right) - \frac{E_a}{RT} \qquad \text{for n = 1} \quad (10)$$

The Ep/Cy/Nc equation of Horowitz-Metzger is given in Eq(11)

$$\ln(1-y) = \frac{E_a(T-T_P)}{R(T_P)} \qquad \text{for n = 1} \quad (11)$$

where T is the absolute temperature, α is the conversion at temperature T, y is the fraction of initial molecules and not yet decomposed, T_{max} is the absolute temperature of maximum reaction rate, β is the rate of heating, A is the frequency factor, DT_{max} is the maximum decomposition temperature, $\theta = T\text{-}DT_{max}$, R is the gas constant and E_a is the activation energy.

The Horowitz model assumes a first order reaction and uses the simplified exponential integrals to obtain the above equation; the Broido model also considers the thermal decomposition process to be a first order reaction. When the Coats-Redfern model was used n=1 was considered for the activation energy calculations.[50] Thus, linear plots were obtained using Broido's method (plotting ln(ln 1/y) *versus* reciprocal of the absolute temperature), the X-R method (In[– (1 – *y*)/T^2] *versus* reciprocal temperature), and the C-R method and ((1 – *y*) *versus* reciprocal temperature) for major degradation events.[51,52] The kinetic analysis for the thermal degradation of both Ep-Cy and Ep-Cy-Nc systems using the Horowitz-Metger model are shown in Fig. 9 (and the kinetic parameters determined from all models are summarised in Table 2). The activation energies values are found to fall in the following order for the models applied: Broido > Horowitz-Metzger > Coats-Redfern.

The activation energies, predicted from the Broido model, for the Ep-Cy systems fall between 237 and 389 kJ/mol, attributed to high thermal stability, due to the formation of an oxazolidinone ring through the epoxy-cyanate co-reaction, leading to a structure with inherently high thermal stability. In the Ep-Cy-Nc systems, the activation energy significantly decreased and found to be in the range 165–381 kJ/mol (using the Broido model). This could be due to the destruction of aliphatic chain present in the clay layers. This interpretation is in agreement with the data obtained for IDT, onset temperature, and char yield for both Ep-Cy and Ep-Cy-Nc systems. The Ep/Cy systems containing functionalized cyanate monomers show higher E_a values and this is in agreement with the TGA data. It is believed that the gaseous oxides of sulphur evolved during the degradation may condense on the remaining polymer, which inhibits the fast degradation of the polymers.

Table 2. The kinetic parameters for the thermal degradation processes

	Models	**Broido**		**Horowitz**		**Coats-Redfern**	
	Kinetic parameters	**E_a (kJ/mol)**	**R^2**	**E_a (kJ/mol)**	**R^2**	**E_a (kJ/mol)**	**R^2**
Ep-Cy systems	Ep-DCBP	249	0.98	222	0.99	198	0.99
	Ep-DCN	266	0.99	243	0.99	219	0.99
	Ep-DCTDP	246	0.99	220	0.99	196	0.99
	Ep-DCDPP	364	0.97	229	0.97	222	0.97
	Ep-DCDPS	248	0.98	204	0.96	181	0.95
Ep-Cy-Nc systems	Ep-DCBP-Nc	175	0.99	157	0.97	134	0.96
	Ep-DCN-Nc	248	0.95	214	0.91	168	0.93
	Ep-DCTDP-Nc	381	0.99	337	0.99	311	0.99
	Ep-DCDPP-Nc	258	0.97	230	0.99	206	0.99
	Ep-DCDPS-Nc	389	0.99	386	0.98	384	0.97

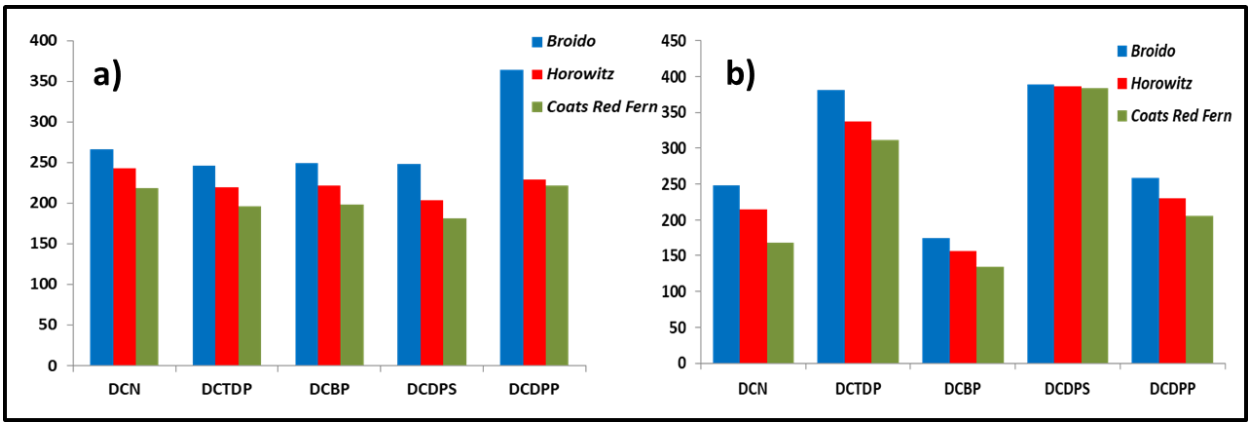

Fig. 9. The plots for the calculation of E_a values for (a) Ep-Cy and (b) Ep-Cy-Nc systems using Horowitz-Metzger model (shown as a function of Cy component)

3.6 Flame retardant properties

While a full analysis of the fire resistance falls outside the scope of this work, a preliminary indication of the flame retardant properties (represented by the limiting oxygen index, LOI, eqn 12) were determined using the empirical formulae proposed by van Krevelen *et al.*[53]. A numerical index (LOI) represents the minimum concentration of oxygen required to just support combustion of a polymer in the air mixture. Thus, higher LOI values represent better flame retardancy.

$$LOI = 17.5 + 0.4CR \qquad (12)$$

where, LOI = limiting oxygen index, and CR = char residue (mass).

The LOI values obtained show a linear relationship with the char yield as shown in Fig. 10. In the first instance, the incorporation of cyanate ester (10 wt%) to the DGEBA-DDS blend, improves the LOI values of the resulting Ep/Cy systems to yield values of 20-23 (compared with a value of 17 % for the base DGEBA-DDS polymer).[54]

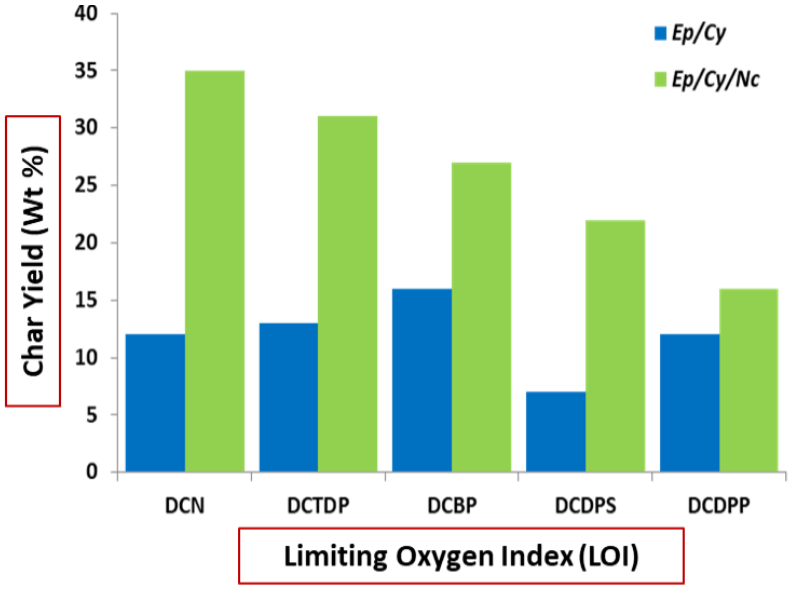

Fig. 10. The correlation study on char yield between Ep-Cy and Ep-Cy-Nc

The Ep-Cy-Nc nanocomposites, which contain both cyanate ester and nanoclays, exhibit LOI values of 22-25. It is generally accepted that empirically determined values of LOI for materials are described as 'flammable' (LOI <20.95), 'slow burning' (LOI<28.0), and 'instrinsically non-flammable' (LOI<100). More specifically, polymers possessing LOI ≥ 20.95, and ≥ 26.0 are considered as 'marginally stable' and 'self-extinguishable' materials respectively.[55-57] Consequently, The epoxy-cyanate copolymers considered in this work, fall into the 'marginally stable' category. The addition of a modest amount of nanoclay clearly increases the flame retardancy in all the epoxy-cyanate blends (and is particularly marked for Ep-DCN-Nc).

3.7 Examination of the fracture properties of the blends

A combination of mechanical tests (using Izod impact strength analysis[58] followed by SEM analysis of the fractured surfaces was performed on the base DGEBA-DDS resin and the Ep-Cy and Ep-Cy-Nc blends. The mechanical data shown (Fig. 11) represent the average of five replicate analyses and when compared with the DGEBA-DDS base system (93 J/m), all the Ep-Cy-Nc systems show increased strength values, due to the synergistic toughening effects of the

cyanate and the nanoclay. For comparison, an Izod value of 18.6 J/m for the cured neat resin homopolymer of the commercial cyanate ester (AroCy B-30) based on bisphenol A has previously been reported[59].

It should be noted that this toughening mechanism is effective as the incorporation of nanoclay into the DGEBA-DDS system already results in a 24% increase in Izod impact strength (115 J/m) for the base system, superior to all but one of the modified Ep-Cy copolymers. The DCN-Ep-Cy-Nc system displays the lowest Izod impact strength, presumably resulting from the non-homogeneous blending with the clay and the rigid aromatic nature of the monomer (the DCBP-Ep-Cy-Nc is similarly affected, with little rotational freedom offered by the direct bond between the aromatic rings). This finding was in agreement with SEM analysis (Fig. 12) where the separation of the clay layers from the matrix resin is seen in the fractured surface of Ep-DCN-Nc. In general, the surfaces show complex features that are typical of shear failure; all the composites show elastic deformation zones that predominate. The poorest performing of the Ep-Cy/Nc systems Ep-DCN-Nc, 102 J/m, and Ep-DCBP-Nc, 109 J/m more isolated nanoclay agglomerations observed on the fracture surfaces of Ep-DCN-Nc and Ep-DCBP-Nc resulted from the processing difficulties caused because of the rigid, planar structural characteristics of naphthalene and biphenyl rings present in the monomers.

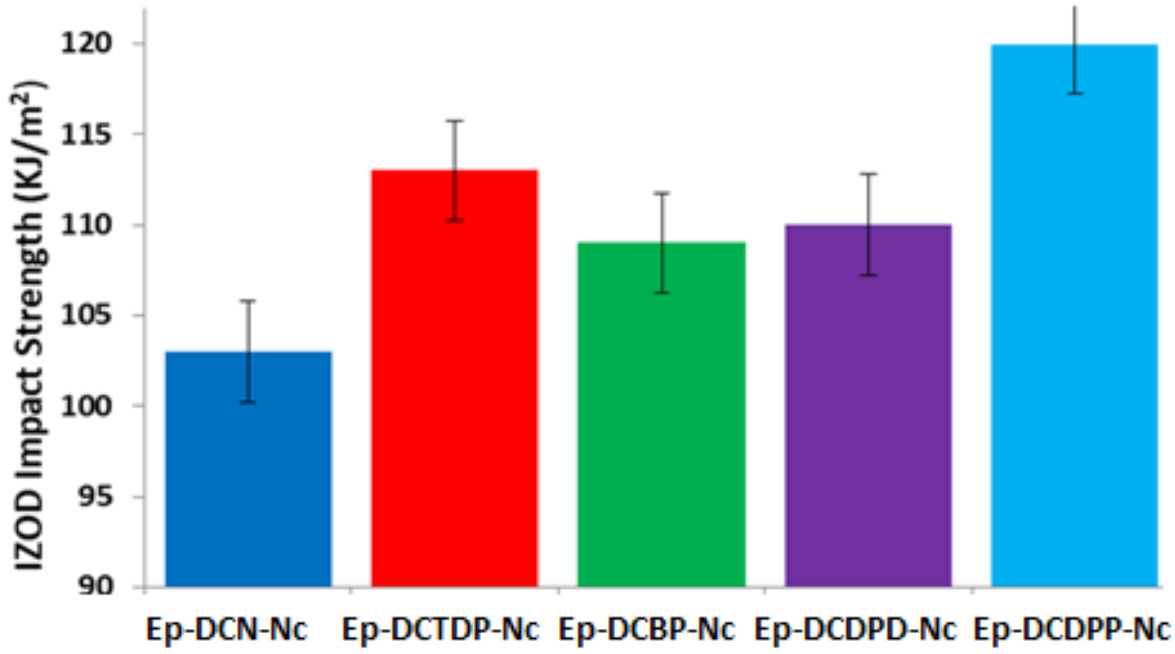

Fig. 11. The impact strength properties of the Ep-Cy-Nc

The SEM images of the fracture surfaces of the cyanate ester systems are shown in fig. 14. All the systems show similar structural patterns because they contain similar kinds of aromatic backbones separating the cyanate ester moieties.

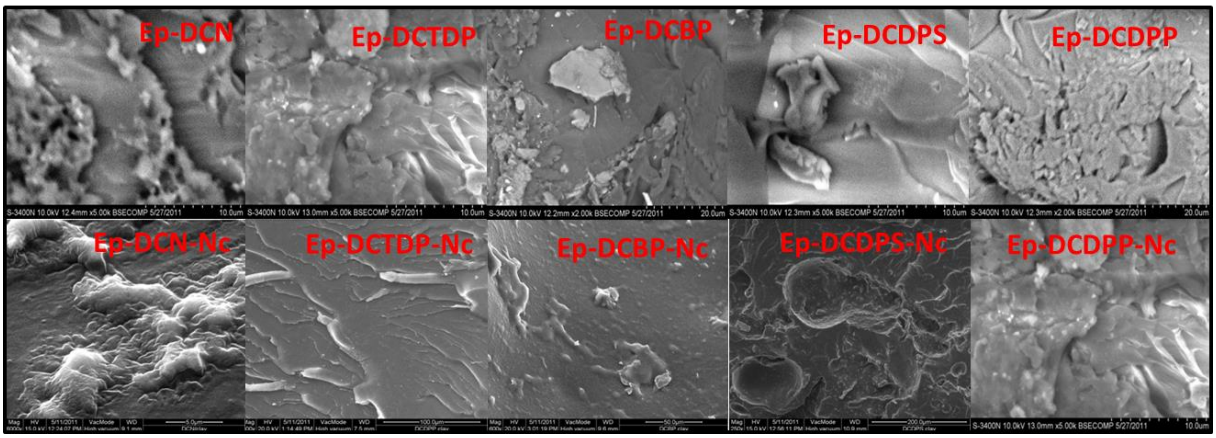

Fig. 12. The scanning electron microscopic images of the cured samples of Ep-Cy and Ep-Cy-Nc systems.

When the fracture surface of the toughened of the samples studied in this work (Ep-DCDPP-Nc, 120 J/m) is examined it displays short, split tails at the crack surface due to the removal of agglomerates between the wave patterns caused by the fracture. The well performing Ep-

DCTDP-Nc system (113 J/m) displays a very complex surface morphology and perhaps the best degree of incorporation of the nanoclay in the matrix. The Ep-DCDPS-Ns system displays cavities at the surface due to the pull out of clay agglomerates and shear failure due to the toughening effect of the nanoclays (resulting in an Izod impact strength of 110 J/m). The appearance of spheroidal cavities confirmed the more ductile nature of the composite during fracture. The single-phase morphology observed in the Ep-DCBP-Nc nanocomposite and the absence of phase separation observed in all the composites confirms the cohesive interaction among the epoxy, cyanate, and nanoclay components. The complete change of morphological structure wrought by the inclusion of nanoclay contributes towards the prevention of linear crack propagation.

4 Conclusions

A series of co-reactive blends comprising a DGEBA-DDS system and various aromatic dicyanates have been prepared and characterized for their thermal behaviour, thermal stability, thermal degradation kinetics, and fracture behaviour morphology. Diffraction data (XRD WAXD analysis) indicate that the clay layers undergo a loss of ordered structure during melt processing, facilitating blending of the nanomaterials within the blends to form nanocomposites. There is a slight penalty in the glass transition temperatures and the onset of thermal degradation in the case of Ep-Cy-Nc systems resulting from intercalation of the nanoclays, as evidenced by the decreased activation energy values determined for the thermal degradation mechanisms. The incorporation of the cyanate to form an oxazolidinone copolymer and nanoclay contribute a synergistic effect in improving the toughness of the resulting nanocomposites and development of more complex morphology. The next phase of the work should involve the incorporation of reinforcement into the best performing of these blends to produce advanced composites.

Acknowledgements

One of the authors (MSL) gives thanks to Dr BSR Reddy, Retired Emeritus Scientist, CSIR-CLRI for his kind support and the MSL is gratefully acknowledges the financial grant received under MMP-06/18 from CSIR-CLRI.

References

1. Kunz-Douglass, S.; Beaumont, P. W.; Ashby, M. F. *J. Mater. Sci*. **1980**, *15*(5), 1109-1123.

2. Jain, P.; Choudhary, V.; Varma, I. K. *J. Macromol. Sci. Polym. Rev*. **2002**, *42*(2), 139–183.

3. Ratna, D.; Manoj, N. R.; Varley, R.; Singh Raman, R. K.; Simon, G. P. *Polym. Int*. **2003**, *52*(9), 1403-1407.

4. Ashrafi, B.; Guan, J.; Mirjalili, V.; Zhang, Y.; Chun, L.; Hubert, P.; Simard, B.; Kingston, C.T.; Bourne, O.; Johnston, A. *Compos. Sci. Technol*. **2011**, *71*(13), 1569-1578.

5. Abdul Khalil, H. P. S.; Jawaid, M.; Firoozian, P.; Zainudin, E. S.; Paridah, M. T. *Int. J. Polym. Anal. Ch.* **2013**, *18*(4), 247-256.

6. Saha, M.; Tambe, P.; Pal, S. *Compos. Interface* **2016**, *23*(3), 255-272.

7. Takao, I.; Takao, K.; Iijima, T.; Kunimi, T.; Oyama, T.; Tomoi, M. *Polym. Int*. **2003**, *52*(5), 773-782.

8. Jiang, X. ; Zhang, Y. ; Zhang, Y. *J. Polym. Sci. Pol. Phys*. **2004**, *42*(7), 1181-1191.

9. Johnsen, B. B.; Kinloch, A. J.; Taylor, A. C. *Polymer* **2005**, *46*(18), 7352-7369.

10. Vyas, A. ; Iroh, J. O. *J. Appl. Polym. Sci*. **2013**, *130*(5), 3319-3327.

11. Chaudhary, S.; Parthasarathy, S.; Mangla, V.; Kumar, D.; Roy, P. K. *Polym. Plast. Technol*. **2015**, *54*(9), 907-915.

12. Kinloch, A. J.; Yuen, M. L.; Jenkins, S. D. *J. Mater. Sci*. **1994**, *29*(14), 3781-3790.

13. Jang, J.; Shin, S. *Polymer* **1995**, *36*(6), 1199-1207.

14. Chaudhary, S.; Surekha, P.; Kumar, D.; Rajagopal, C.; Roy, P. K. *Polym. Compos*. **2015**, *36*(1), 174-183.

15. Heng, Z.; Chen, Y.; Zou, H.; Liang, M. *RSC Adv*. **2015**, *5*(53), 42362-42368.

16. Iredale, R. J.; Ward, C.; Hamerton, I. *Prog. Polym. Sci*. **2017**, *69*, 1-21.

17. Fang, T.; Shimp, D. A. *Progress Polym. Sci*. **1995**, *20*(1), 61-118.

18. Gaina, V., and Gaina, C. *Polym. Plast. Technol*. **2009**, *48*(5), 525-529.

19. Abed, J. C.; Mercier, R.; Mcgrath, J. E. *J. Polym. Sci. Part A: Polym. Chem*. **1997**, *35*(6), 977-987.

20. Dinakaran, K.; Kumar, R. S.; Alagar, M. *Mater. Manuf. Process*. **2005**, *20*(2), 299-315.

21. Hamerton, I. In Chemistry and Technology of Cyanate Ester Resins, I. Hamerton (Ed.); Blackie Academic and Professional: Glasgow, **1994**; pp. 1-6.

22. Shimp, D. A.; Chin, B. In Chemistry and Technology of Cyanate Ester Resins; Hamerton, I., Ed.; Blackie Academic and Professional: Glasgow, **1994**; pp. 231−257.

23. Nagendiran, S.; Chozhan, C. K.; Alagar, M.; Hamerton, I. *High Perform. Polym*. **2008**, *20*(3), 323-347.

24. Chandrasekaran, S.; Duoss, E. B.; Worsley, M. A.; Lewicki, J. P. *J. Mater. Chem. A*. **2018** *6*(3), 853-858.

25. Compton, B. G.; Lewis, J. A. *Adv. Mater*. **2014**, *26*(34), 5930-5935.

26. Kokkinis, D.; Schaffner, M.; Studart, A. R. *Nat. Comm*. **2015**, *6*, 8643.

27. Kuang, X.; Zhao, Z.; Chen, K., Fang, D.; Kang, G.; Qi, H. J. *Macromol. Rapid Comm*. **2018**, *39*(7), 1700809.

28. Rolland, J. P. J. *Photopolym. Sci. Technol*. **2016**. *29*(3), 451-452.

29. Ivanov, D. S.; White, J. A.; Hendry, W.; Mahadik, Y.; Minett, V.; Patel, H.; Ward, C. *Adv. Manuf. Polym. Compos. Sci*. **2015**, *1*(1), 26-35.

30. Stanier, D.; Radhakrishnan, A.; Gent, I.; Roy, S.S.; Hamerton, I.; Potluri, P.; Scarpa, F.; Shaffer, M.; Ivanov, D.S. *Compos. Struct.* **2019**, *207*, 72-80.

31. Grigat E.; Pütter R. *Chem. Ber*. **1964**, *97*, 3022-3026.

32. Lakshmi M. S.; Srividhya, M.;. Reddy B. S. R. *J. Polym. Res.* **2003**, *10*, 259-266.

33. Lee, J. Y.; Jang, J. *J Polym. Sci. Part A: Polym. Chem*. **1999**, *37*, 419.

34. Shimp, D.A., Wentworth, J.E. *Int*. *SAMPE Symp*. **1992**, *37*, 293-305.

35. Bauer, M., Tänzer, W., Munch, H.; Ruhman, R. *Acta Polym*. **1989**, *40*, 335.

36. Bauer, M.; Bauer, J.; R Ruhman R.; Kühn, G. *Acta Polym.* **1989**, *40*, 397.

37. Wang, C. S.; Leu, T. S.; Hsu, K. R. *Polymer* **1998**, *39*, 2921.

38. Wang, C. S.; Lee, M. C. *Polymer* **2000**, *41*, 3631.

39. Hamerton, I.; Heald, C. R.; Howlin, B. *J. Macromol. Theor. Simul*. **1996**, *5*, 305-320.

40. Yan, H. Q.; Chen, S.; Qi, G.-R. *Polymer* **2003**, *44*, 7861-7867.

41. Ramirez, M. L.; Walters, R.; Lyon, R. E.; Savitski, E. P. *Polym. Degrad. Stab*. **2002**, *78*, 73-82.

42. Hamerton, I.; Emsley, A. M.; Howlin, B. J.; Klewpatinond, P.; Takeda, S. *Polymer* **2003**, *44*(17), 4839-4852.

43. Hamerton, I. Ph.D. Thesis, University of Surrey, **1991**.

44. Bauer, R.S. Epoxy Resin Chemistry. Advances in Chemistry, ACS Symposium Series, American Chemical Society: Washington, DC, **1979**, 114.

45. Doyle, C.D. *Anal. Chem*. **1961**, *33*, 77–79.

46. Pashaei, S.; Avval, M. M.; Syed, A. A.; *Chem. Ind. Chem. Eng. Q*. **2011**, *17*(2), 141-151.

47. Holubka J. W.; Devries J. E.; Dickie R. A. *Ind. Eng. Chem. Prod. Res. Dev.* **1984**, *23*, 63-70.

48. Raudenbush, W. In R. S. Bauer, Eds.; ACS Symposium: Washington D.C., **1979**. Ser. 114.

49. Al-Mulla, A.; Shaban H. I. *Int. J. Polym Mater*. **2008**, *57*(3), 275-287.

50. Muralidhara, K. S., and Sreenivasan, S. *World Appl. Sci. J*, **2010**, *11*(2), 184-189.

51. Ashok, M. A.; Achar B. N. *Indian Acad. Sci. (Mater. Sci.)*. **2008**, *31*(1), 29-35.

52. Muralidhara, K. S.; Sreenivasan, S. J. *Sci. Ind. Res.* **2010**, 69, 879-885.

53. Van Krevelen, D. W. *Polymer* **1975**, *16*, 615–620.

54. Schartel, B.; Braun, U.; Balabanovich, A.I.; Artner, J.; Ciesielski, M.; Döring, M.; Perez, R.M.; Sandler, J.K.W.; Altstädt, V.*Eur. Polym. J*. **2008**, *44*(3), 704-715.

55. Nelson, M. I. *Combust. Theor. Model*. **2001**, *5*, 59-83.

56. Horrocks, A. R.; Tunc, M.; Price, D. *Text. Prog*. **1989**, *18*(1-3) 1-205.

57. Fenimore, C. P. In Flame-retardant polymeric materials; M. Lewin, M.; Atlas, S. M.; Pearce, E. M., Eds.; Plenum: New York, **1975**; Vol. 1, pp 371-397.

58. Wu, H.; Krifa, M.; Koo, J. H. *Polym. Plast. Technol. Eng*. **2018**, *57*(8), 727-739.

59. Ganesan, G.; Muthusamy, S. *Polym. Compos.* **2009**, *30*(6), 782-790.